Photon-counting CT: high-resolution imaging of coronary stents

Mannil, Manoj ; Hickethier, Tilman ; von Spiczak, Jochen ; Baer, Matthias ; Henning, André ; Hertel, Madeleine ; Schmidt, Bernhard ; Flohr, Thomas ; Maintz, David ; Alkadhi, Hatem

Abstract: PURPOSE: The aim of this study was to investigate computed tomography (CT) imaging characteristics of coronary stents using a novel photon-counting detector (PCD) in comparison with a conventional energy-integrating detector (EID). MATERIALS AND METHODS: In this in vitro study, 18 different coronary stents were expanded in plastic tubes of 3 mm diameter, were filled with contrast agent (diluted to an attenuation of 250 Hounsfield units [HU] at 120 kVp), and were sealed. Stents were placed in an oil-filled custom phantom calibrated to an attenuation of -100 HU at 120 kVp for resembling pericardial fat. The phantom was positioned in the gantry at 2 different angles at 0 degree and 90 degrees relative to the z axis, and was imaged in a research dual-source PCD-CT scanner. Detector subsystem "A" used a standard 64-row EID, while detector subsystem "B" used a PCD, allowing high-resolution scanning (detector pixel-size 0.250 × 0.250 mm in the isocenter). Images were obtained from both detector systems at identical tube voltage (100 kVp) and tube current-time product (100 mA), and were both reconstructed using a typical convolution kernel for stent imaging (B46f) and using the same reconstruction parameters. Two independent, blinded readers evaluated in-stent visibility and measured noise, intraluminal stent diameter, and in-stent attenuation for each detector subsystem. Differences in noise, intraluminal stent diameter, and in-stent attenuation where tested using a paired t test; differences in subjective in-stent visibility were evaluated using a Wilcoxon signed-rank test. RESULTS: Best results for in-stent visibility, noise, intraluminal stent diameter, and in-stent attenuation in EID and PCD were observed at 0-degree phantom position along the z axis, suggesting higher in-plane compared with through-plane resolution. Subjective in-stent visibility was superior in coronary stent images obtained from PCD compared with EID ($P < 0.001$). Mean in-stent diameter was 28.8% and 8.4% greater in PCD (0.85 ± 0.24 mm; 0.83 ± 0.14 mm) as compared with EID acquisitions (0.66 ± 0.21 mm; 0.76 ± 0.13 mm) for both 0-degree and 90-degree phantom positions, respectively. Average noise was significantly lower ($P < 0.001$) for PCD (5 ± 0.2 HU) compared with EID (8.3 ± 0.2 HU). The increase in in-stent attenuation (0 degree: Δ 245 ± 163 HU vs Δ 156.5 ± 126 HU; $P = 0.006$; 90 degrees: Δ 194 ± 141 HU vs Δ 126 ± 78 HU; $P = 0.001$) was significantly lower for PCD compared with EID acquisitions. CONCLUSIONS: At matched CT scan protocol settings and identical image reconstruction parameters, the PCD yields superior in-stent lumen delineation of coronary artery stents as compared with conventional EID arrays.

DOI: https://doi.org/10.1097/RLI.0000000000000420

Mannil, Manoj; Hickethier, Tilman; von Spiczak, Jochen; Baer, Matthias; Henning, André; Hertel, Madeleine; Schmidt, Bernhard; Flohr, Thomas; Maintz, David; Alkadhi, Hatem (2018). Photon-counting CT: high-resolution imaging of coronary stents. Investigative Radiology, 53(3):143-149.
DOI: https://doi.org/10.1097/RLI.0000000000000420

Photon-Counting CT
High-Resolution Imaging of Coronary Stents

Manoj Mannil, MD, MSc, Tilman Hickethier, MD,† Jochen von Spiczak, MD, MSc,* Matthias Baer, PhD,‡ André Henning, MSc, MSc,‡ Madeleine Hertel, BSc,‡ Bernhard Schmidt, PhD,‡§ Thomas Flohr, PhD,‡ David Maintz, MD,† and Hatem Alkadhi, MD, MPH, EBCR**

Purpose: The aim of this study was to investigate computed tomography (CT) imaging characteristics of coronary stents using a novel photon-counting detector (PCD) in comparison with a conventional energy-integrating detector (EID).

Materials and Methods: In this in vitro study, 18 different coronary stents were expanded in plastic tubes of 3 mm diameter, were filled with contrast agent (diluted to an attenuation of 250 Hounsfield units [HU] at 120 kVp), and were sealed. Stents were placed in an oil-filled custom phantom calibrated to an attenuation of −100 HU at 120 kVp for resembling pericardial fat. The phantom was positioned in the gantry at 2 different angles at 0 degree and 90 degrees relative to the *z* axis, and was imaged in a research dual-source PCD-CT scanner. Detector subsystem "A" used a standard 64-row EID, while detector subsystem "B" used a PCD, allowing high-resolution scanning (detector pixel-size 0.250 × 0.250 mm in the isocenter). Images were obtained from both detector systems at identical tube voltage (100 kVp) and tube current-time product (100 mA), and were both reconstructed using a typical convolution kernel for stent imaging (B46f) and using the same reconstruction parameters. Two independent, blinded readers evaluated in-stent visibility and measured noise, intraluminal stent diameter, and in-stent attenuation for each detector subsystem. Differences in noise, intraluminal stent diameter, and in-stent attenuation where tested using a paired *t* test; differences in subjective in-stent visibility were evaluated using a Wilcoxon signed-rank test.

Results: Best results for in-stent visibility, noise, intraluminal stent diameter, and in-stent attenuation in EID and PCD were observed at 0-degree phantom position along the *z* axis, suggesting higher in-plane compared with through-plane resolution. Subjective in-stent visibility was superior in coronary stent images obtained from PCD compared with EID ($P < 0.001$). Mean in-stent diameter was 28.8% and 8.4% greater in PCD (0.85 ± 0.24 mm; 0.83 ± 0.14 mm) as compared with EID acquisitions (0.66 ± 0.21 mm; 0.76 ± 0.13 mm) for both 0-degree and 90-degree phantom positions, respectively. Average noise was significantly lower ($P < 0.001$) for PCD (5 ± 0.2 HU) compared with EID (8.3 ± 0.2 HU). The increase in in-stent attenuation (0 degree: Δ 245 ± 163 HU vs Δ 156.5 ± 126 HU; $P = 0.006$; 90 degrees: Δ 194 ± 141 HU vs Δ 126 ± 78 HU; $P = 0.001$) was significantly lower for PCD compared with EID acquisitions.

Conclusions: At matched CT scan protocol settings and identical image reconstruction parameters, the PCD yields superior in-stent lumen delineation of coronary artery stents as compared with conventional EID arrays.

Key Words: photon-counting, CT, detector, coronary artery stents, spatial resolution

(*Invest Radiol* 2017;00: 00–00)

Received for publication June 6, 2017; and accepted for publication, after revision, August 27, 2017.

From the *Institute of Diagnostic and Interventional Radiology, University Hospital Zurich, University of Zurich, Zurich, Switzerland; †Department of Radiology, University Hospital of Cologne, Cologne; ‡Siemens Healthcare GmbH, Forchheim; and §Institute of Medical Physics, University Erlangen-Nürnberg, Erlangen, Germany.

The authors report no conflicts of interest.

Correspondence to: Hatem Alkadhi, MD, MPH, EBCR, Institute of Diagnostic and Interventional Radiology, University Hospital Zurich, Raemistr. 100, CH-8091 Zurich, Switzerland. E-mail: hatem.alkadhi@usz.ch.

ISSN: 0020-9996/17/0000–0000
DOI: 10.1097/RLI.0000000000000420

Percutaneous coronary intervention (PCI) is the most frequently performed medical intervention worldwide. Approximately 1.5 million patients undergo PCI in the United States per year.[1] Although the use of balloon angioplasty is limited by abrupt vessel closure owing to dissections and restenosis, coronary stents have the capacity to overcome these shortcomings at increased procedural safety and efficacy.[2] However, stent-mediated arterial injuries may elicit neointimal hyperplasia, leading to in-stent restenosis (ISR) requiring repeat vascularization in up to one third of patients.[3] Even in case of drug-eluting stents, ISR occurs in approximately 10% of patients.[4] Other complications include in-stent thrombosis and stent fractures, which are predisposing factors for ISR. Because approximately 50% of patients with significant ISR are asymptomatic and PCI is associated with high costs and low, albeit non-negligible, periprocedural risk,[5] cost-effective and noninvasive imaging techniques are desirable.

From all noninvasive imaging modalities, computed tomography (CT) of the coronary artery system represents the most promising one, owing to continuous technological advances including the temporal and spatial resolution in the past years.[6–8] Still, the conventional evaluation of stents and specifically of ISR remains challenging due to metal artifacts, blooming, photon starvation, beam hardening, and partial volume effects.[9,10] All these factors lead to reduced visualization of the true in-stent lumen, and it was estimated that approximately 12% of all coronary stents cannot be imaged with a diagnostic quality.[11] This is reflected in current guidelines that do not recommend routine coronary CT imaging for stent lumen visualization in general, but only in patients with a left main coronary artery stent and in stents being ≥ 3 mm in diameter.[12,13]

Novel CT scanner developments have introduced photon-counting detector (PCD) technology, where semiconductor materials such as cadmium telluride (CdTe) convert x-rays directly into electric signal pulses. Each incoming x-ray quantum generates clouds of free charge proportional to the energy of the incident x-ray beam. An electrical field inside the detector material transports the charge clouds to anode pixels in which electrical current is induced. Highly integrated circuits transform these charge pulses to voltage pulses of a few nanosecond duration that will be digitally counted. For limiting the amount of data delivered by the detector, it is common practice to stratify the registered photons within certain energy ranges or "energy bins" and to read only data for each of the bins. Therefore, PCD technology differs from current energy-integrating detectors (EIDs) by counting individual photons and allocating them to predetermined energy thresholds and bins.[14] An additional potential advantage of PCD systems is their improved spatial resolution that can be achieved due to smaller detector pixels as compared with conventional EID systems. In contrast to conventional EID systems, PCDs implement a direct conversion of the incoming photon flux into an electrical signal. Because of this direct conversion, PCDs possess higher dose efficiency at smaller detector pixels compared with EIDs at same pixel sizes. Because of their indirect conversion technique, EIDs need optically intransparent separation layers that block optical photons between each detector pixel. X-ray photons hitting these separation layers do not contribute to the measured signal and decrease the dose efficiency of EIDs. Because the blocking area does not scale with

the pixel size, the difference between PCDs and EIDs in terms of dose efficiency increases with decreasing pixel size. As a consequence, the PCD technology used in the prototype scanner offers an ultra-high-resolution ("SHARP" mode) imaging technique with an effective detector size of 0.25 × 0.25 mm at the isocenter, compared with the 0.5 × 0.5 mm of the standard "MACRO" mode of the PCD, and 0.50 to 0.625 mm on commercial EIDs.[15] Although recent studies demonstrated the image quality of the PCD technology to be comparable to that of current state-of-the-art CT scanners with integrating detectors,[16–18] the issue of high spatial resolution imaging with PCD technology, however, was not investigated so far.

The hypothesis of our study was that the PCD would improve the image quality and in-stent visualization of coronary artery stents. Thus, we investigated quantitative and qualitative CT imaging characteristics of coronary artery stents using a PCD system in comparison with a conventional EID at matched data acquisition and image reconstruction parameters.

MATERIALS AND METHODS

Experimental Setup

Eighteen different coronary artery stents with different material composition were examined in this in vitro study. Table 1 summarizes names, manufacturers, materials, diameters, lengths, and strut-thicknesses. Sixteen coronary stents (88%) were made of stainless surgical steel (316L), of which 3 (19%) had an additional tantalum coating, 2 (13%) carbon coating with platinum markers, and 2 (13%) gold coating. The remaining 2 stents were made of either cobalt-chrome (6%) or cobalt alloy with titanium coating (6%).

Before imaging, each stent was expanded in a coronary vessel phantom made of a plastic tube with an inner diameter of 3 mm to simulate the coronary artery. The plastic material had a thickness of less than 0.3 mm, and its CT attenuation was similar to that of a vessel wall (35 Hounsfield units [HU]). The tube was filled with contrast medium (Accupaque 350, 350 mg/mL, GE Healthcare, Chicago, IL), diluted to a density of 250 HU at 120 kVp, and sealed airtight at both ends. Three tubes at a time were then placed in a synthetic container filled with low-viscosity engine oil. The density of the oil was titrated to −100 HU at 120 kVp by adding Lipiodol Ultrafluid (Guerbet, Cedex, France) to simulate the attenuation of epicardial fat. The phantom (Fig. 1) was then positioned in the isocenter of the CT gantry at 2 different angles (0 degree and 90 degrees) relative to the scanner's *z* axis.

CT Data Acquisition and Postprocessing

CT data acquisition was performed using a modified second-generation 64-row, 128-section dual-source CT scanner (SOMATOM Definition Flash; Siemens Healthcare GmbH, Erlangen, Germany), which was equipped with both a conventional EID and a novel PCD. The primary difference between the commercial system and this research scanner system was the replacement of 1 of the 2 dual-source scanner's EID arrays with 1 CdTe-based PCD array, which allows high-resolution scanning at 2 energy thresholds.

The PCD-CT system was composed of 1.6-mm-thick CdTe semiconducting sensors. For stent measurements on PCD system-derived images, the "SHARP" mode was used for data acquisition. In the "SHARP" mode, 2 × 2 subpixels (2 subpixels in axial and 2 subpixels in *z* direction) of the PCD are combined to 1 single "SHARP" pixel. The pixel pitch of the subpixels is 0.225 mm, and the resulting pixel pitch of the SHARP pixels is therefore 0.450 mm (at the detector). To reduce in-plane scatter intensities and artifacts, the PCD is equipped with a 1-dimensional antiscatter collimator grid[19] whose grid lamellae have a pitch of 0.9 mm. The effective pixel size at the isocenter was 0.25 × 0.25 mm (*axial direction* × *z-direction*) in the "SHARP" mode. Each subpixel of the PCD array provides 2 energy thresholds: the lower threshold T_L is adjustable in a range from 20 to 50 keV, and the higher threshold T_H is adjustable in a range from 50 to 90 keV. For comparison with conventional EID, the lower threshold in PCD was set to 25 keV and the energy-resolved readout of the PCD array was performed in the "SHARP" mode.[14]

A major advantage of the setup of the PCD prototype scanner was that the phantom did not need to be repositioned between scans, but was kept at identical positions between scans with the EID and the PCD. Image data were obtained with fixed tube voltage (100

TABLE 1. Coronary Stent Characteristics

Name	Manufacturer	Material	Diameter, mm	Length, mm	Strut-Thickness, mm
Pura AL16	Devon Medical	Stainless steel 316L	3	16	0.08
ApoloBionert	Iberhospitex	Stainless steel 316L (treated with O2 ion jets)	3	14	0.115
CCSV	Micro Science Medical	Stainless steel 316L (tantalum coating)	3	16	0.6–0.8
Coroflex Delta	B. Braun	Stainless steel 316L	3	16	0.12
Magic Wallstent	Boston Scientific	Cobalt alloy with titanium core (33%)	4	32	0.1
MSM Coronary	Micro Science Medical	Stainless steel 316L (tantalum coating)	3	26	0.08
NIR Royal	Boston Scientific	Stainless steel 316LS (gold coating)	3	25	0.14
NIR Royal Adv	Boston Scientific	Stainless steel 316LS (gold coating)	3	15	0.11
Palmaz	Cordis	Stainless steel 316L	3	14	0.07–0.095
Pixel	Guidant	Stainless steel 316L	3	23	0.1
R-Stent	Orbus Medical Technologies	Stainless steel 316L	3	25	0.1–0.127
SonicBx	Cordis	Stainless steel 316L	3	18	0.14
Syncro	Sorin Biomedica	Stainless steel 316L (carbon coating and 2 platinum markers)	3	19	0.075
Tecnic	Sorin Biomedica	Stainless steel 316L (carbon coating and 2 platinum markers)	3	19	0.075
Tetra	Guidant	Stainless steel 316L	3	13	0.09–0.12
Ultra	Guidant	Stainless steel 316L	3	18	0.128
Vision Multi Link	Abbott Vascular Devices	Cobalt-chrome	3	15	0.08
ZoMaxx	Abbott Vascular Devices	Stainless steel 316L (tantalum coating)	3	15	0.115

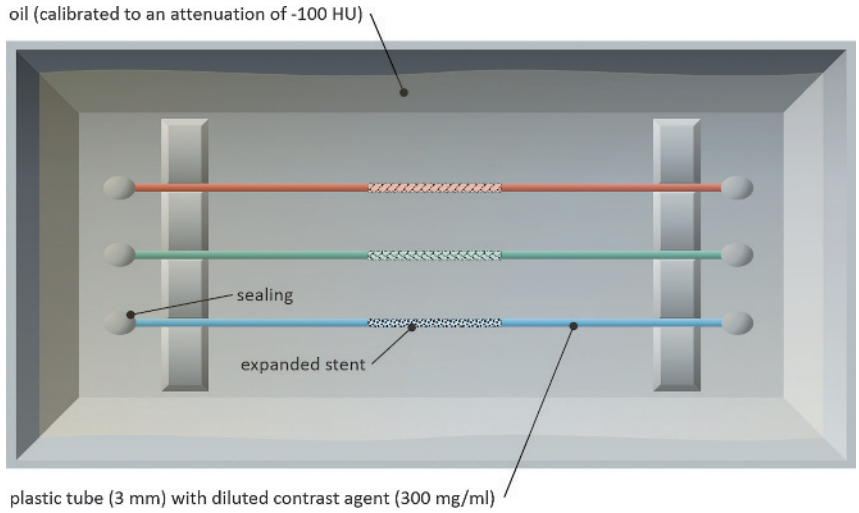

FIGURE 1. Schematic representation of the phantom setup. Three coronary stents at a time were expanded within plastic tubes of 3 mm diameter, filled with contrast medium, and positioned in the oil-filled synthetic container. The stents were placed at different levels of the phantom to avoid interleaving artifacts. The phantom was then positioned in the isocenter of the CT gantry at both 0 degree and 90 degrees along the *z* axis.

kVp) and tube current-time product (100 eff. mA) without using automated tube current modulation. Further scanning parameters are depicted in Table 2.

For a direct comparison between PCD and EID in a typical clinical setup, raw data from the 2 detectors were reconstructed with identical slice thickness of 0.6 mm, increment of 0.3 mm, field of view of 150 × 150 mm^2, image matrix (512 × 512 each), and using the same convolution kernel B46 (typical kernel for stent imaging). The resolution of the B46 kernel is well below the intrinsic resolution of the PCD. Therefore, the images reconstructed with the B46 will have a similar resolution regardless whether the raw data were acquired by the PCD or EID, because the target modulation transfer function of B46 is the same in both cases. Theoretically, the higher intrinsic resolution of the PCD (smaller detector pixels) should convert into a reduction of image noise as compared with the EID. In addition, the image quality of the PCD images profits from improved in-plane and through-plane sampling due to the smaller detector pixels.

After image reconstruction, all data were transferred for readout to our hospital's picture archiving and communication system (IMPAX, Agfa, Version 6.6.1; Mortsel, Belgium).

Image Analysis

Both CT image data sets (conventional EID and PCD) were analyzed twice by the same reader (R1, with 4 years of cardiovascular imaging experience), with a time interval between readouts of 3 weeks to avoid recall bias. A second, independent reader (R2, with 2 years of experience in cardiovascular imaging) analyzed the image data sets separately for determining the interreader reliability. Both readers were blinded to the imaging mode and stent type.

Qualitative Readout

Overall image quality of conventional EID and PCD images was assessed using a subjective 3-point Likert scale (1 = excellent; 2 = moderate, still diagnostic; 3 = insufficient, nondiagnostic). The visibility of the coronary in-stent lumen was assessed on axial images using a subjective 3-point Likert scale (1 = in-stent lumen not delineated due to severe artifacts; 2 = partially delineated, moderate quality; 3 = delineated with good quality), as previously described.[20]

Quantitative Readout

All quantitative analyses were performed at a fixed window width of 1500 HU and window center of 300 HU, as previously shown.[21] In-stent diameter measurements of the coronary stents in EID and PCD images were performed using a caliper tool in open-source image processing software (ImageJ 1.47 t, National Institute of Health, United States). Measurements at 3 different in-stent locations were averaged to account for differences in stent strut positions. Differences between the measured and reported true in-stent diameter were defined as follows: in-stent diameter difference = [inner diameter of plastic tube − (2 × strut thickness)] − measured in-stent diameter.

Image noise was defined as the standard deviation of the CT numbers (in Hounsfield units) in a region of interest (ROI) placed in the oil adjacent to the stents (average ROI size, ~20 cm^2).

Delta (Δ) in-stent CT attenuation values were obtained by use of rectangular ROIs on longitudinally reformatted images (average of 3 measurements). The ROIs for these measurements were placed to be as large as possible, while carefully avoiding stent struts or blooming artifacts at the same time. Furthermore, the CT numbers proximal and distal to the coronary stent, inside the plastic tube, were averaged. The difference in attenuation across the stent was calculated as follows: Δ in-stent attenuation = in-stent CT number − CT number outside the stent.[20] Averaged CT attenuation intensity profiles in stent images of both detectors were analyzed placing a straight line in the stent lumen. Results of all 18 stents were averaged according to detector type and plotted against phantom tube length.

TABLE 2. CT Data Acquisition Modes

	Acquisition	Rotation Time	Pitch	$CTDI_{vol}$ (32 cm)
EID	2 × 64 × 0.6 mm (with z flying focal spot)	0.5 s	0.6	4.1 mGy
PCD	48 × 0.25 mm	0.5 s	0.6	5.1 mGy

$CTDI_{vol}$ indicates computed tomography dose index volume; EID, energy-integrating detector; PCD, photon-counting detector.

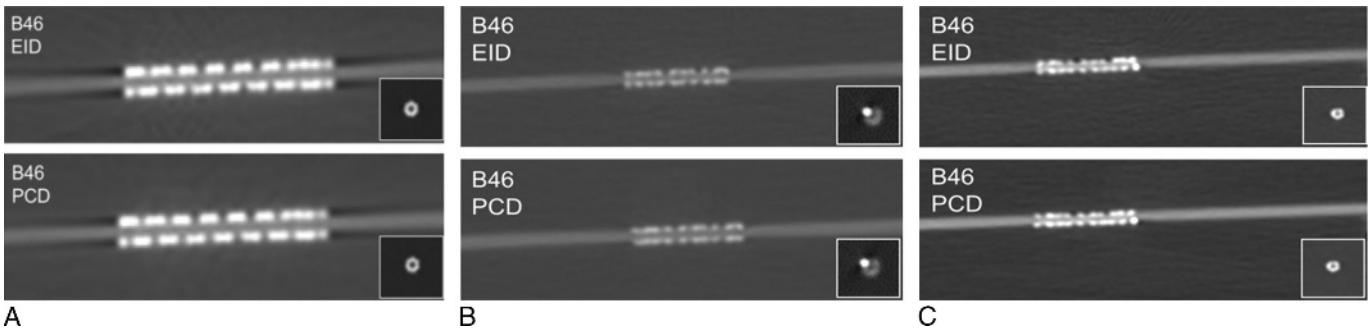

FIGURE 2. Coronal and axial CT images of 3 representative coronary stents ([A] Boston Scientific, NIR Royal; [B] Sorin Biomedica Tecnic; and [C] Sorin Biomedica Syncro) imaged with a conventional EID and a PCD detector at identical tube voltage, tube current, slice thickness, reconstruction kernel, and at similar window settings. PCD images show decreased image noise and less metal artifacts adjacent to the stent struts.

Statistical Analysis

Continuous variables were expressed as means ± standard deviation, and categorical variables as frequencies or percentages. Normal distribution of continuous data was confirmed by use of the Kolmogorov-Smirnoff test.

The intrareader and interreader agreement for qualitative imaging parameters (image quality, visibility of in-stent lumen) was calculated by using Cohen's kappa. The intrareader and interreader agreement regarding quantitative imaging parameters in-stent diameter measurements of the coronary stents in EID and PCD images, image noise, CT attenuation, and lumen measurements were analyzed by using intraclass correlation coefficients. According to Landis and Koch,[22] values of 0.61 to 0.80 were interpreted as substantial, and 0.81 to 1.00, as excellent agreement.

Although mean differences of qualitative imaging parameters (image quality, visibility of in-stent lumen) between EID and PCD images were tested using a Wilcoxon signed rank test, mean differences in quantitative imaging parameters (in-stent diameter, image noise, and in-stent attenuation) were tested using a paired Student *t* test.

A 2-tailed *P* value below 0.05 was inferred to indicate significance. All statistical analyses were conducted using commercially available software (SPSS, release 23.0; IBM, Chicago, IL).

RESULTS

Intrareader and Interreader Agreement

At a phantom position of 90 degrees along the *z* axis, overall image quality had a substantial intrareader and interreader agreement for EID (0.75 and 0.6, respectively) and for PCD images (0.77 and 0.6, respectively). Assessment of in-stent visibility had a substantial intrareader and interreader agreement for EID (0.7 and 0.67) and for PCD images (0.68 and 0.67, respectively). All quantitative parameters showed substantial to excellent intrareader/interreader agreement, at a range of 0.9–0.99/0.81–0.96 for EID and 0.8–0.99/0.7–0.95 for PCD.

At a phantom position of 0 degree along the *z* axis, overall image quality had a substantial intrareader and interreader agreement for EID (0.7 and 0.62, respectively) and for PCD images (0.6, both). Assessment of in-stent visibility had a substantial intrareader and interreader agreement for EID (0.65 and 0.6) and for PCD images (0.7 and 0.6, respectively). All quantitative measurements showed excellent intrareader/interreader agreement, at a range of 0.94–0.99/0.84–0.89 for EID and 0.95–0.99/0.81–0.97 for PCD.

Qualitative Results

At a phantom position of 0 degree, excellent image quality was observed in 12 (67%) of 18 stents in EID images and in 15 (83%) of

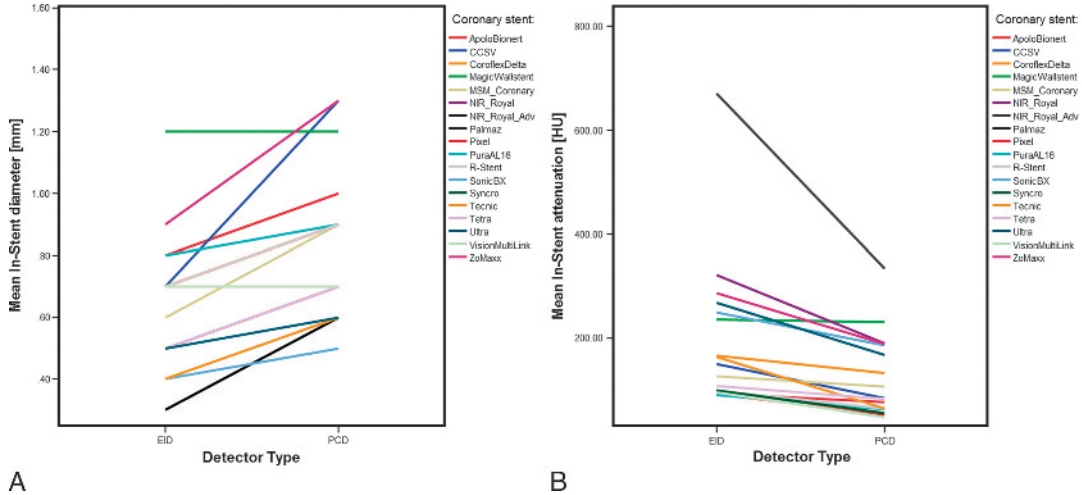

FIGURE 3. Line diagram depicting differences in (A) mean in-stent diameter, and (B) mean in-stent attenuation between EID and PCD images. PCD images of coronary stents achieve significantly higher in-stent diameter ($P < 0.001$), whereas mean in-stent attenuation values ($P < 0.001$) are significantly lower in comparison to conventional EID imaging.

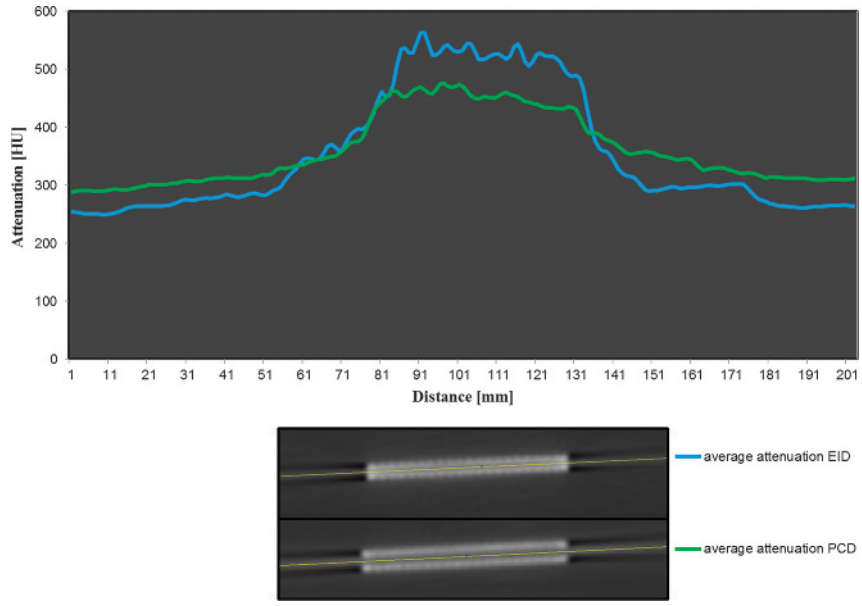

FIGURE 4. A, Averaged CT attenuation intensity profiles of all 18 stents at 90-degree phantom position of EID (blue) and PCD (green) images. PCD CT measurements result in significantly lower in-stent attenuation values compared with EID measurements. B, Example of intraluminal attenuation measurements in CT images of a coronary artery stent of 3 mm diameter (Boston Scientific, Magic Wallstent, not to scale) using a (above) conventional energy-integrating detector (EID), and (below) a photon-counting detector (PCD) at identical tube voltage, current, slice thickness, reconstruction kernel, and window settings. Note the markedly decreased intraluminal diameter in EID, compared with PCD imaging. This observation is likely due to the decreased blooming artifacts in EID imaging.

18 stents in PCD images. No coronary stent image quality in either image data set was graded as insufficient/nondiagnostic. Identical findings of image quality were observed at 90-degree phantom position along the *z* axis: excellent image quality was rated in the same 12 (67%) of 18 coronary stents in EID images and 15 (83%) of 18 stents with PCD images. Again, no coronary stent image quality in either image data set was graded as insufficient/nondiagnostic.

At both phantom positions (0 degree and 90 degrees), subjective in-stent visibility was superior in stent images obtained with PCD compared with the EID array ($P < 0.001$). Representative images of a 3-mm stainless steel stent with gold coating obtained with the PCD and EID array are provided in Figure 2.

Quantitative Results

At a 0-degree phantom position, mean intraluminal stent diameter was 28.8% greater in PCD (0.85 ± 0.24 mm) compared with EID images (0.66 ± 0.21 mm; $P < 0.001$). Stent diameters were significantly lower for PCD compared with EID (1.9 ± 0.1 mm vs 2.1 ± 0.08 mm; $P < 0.001$) (Fig. 3).

At 90-degree phantom position, mean intraluminal stent diameter was 8.4% greater in PCD (0.83 ± 0.14 mm) compared with EID images (0.76 ± 0.13 mm; $P = 0.006$). Stent diameters did not differ significantly (EID: 1.99 ± 0.4 mm; PCD: 1.98 ± 0.4 mm; $P = 0.9$).

Average image noise was significantly lower for PCD (5 ± 0 HU) as opposed to EID images (8 ± 0 HU; −37.5%; $P < 0.001$).

At 0-degree phantom position, Δ in-stent attenuation (245 ± 163 HU vs 156.5 ± 126 HU; $P = 0.006$) was significantly lower for PCD compared with EID images. In detail, mean intraluminal attenuation was 709 ± 161 HU for EID and 629 ± 125 HU for PCD. Mean out-of-stent attenuation was 455 ± 21 HU proximal and 473 ± 19 HU distal to the stent for EID, as well as 467 ± 29 HU proximal and 478 ± 29 HU distal to the stent for PCD, respectively.

At 90-degree phantom position, Δ in-stent attenuation (194 ± 141 HU vs 126 ± 78 HU; $P = 0.001$) were significantly lower for PCD compared with EID images. In detail, mean intraluminal attenuation was 462 ± 141 HU for EID, and 434 ± 104 HU for PCD. Mean out-of-stent attenuation was 262 ± 48 HU proximal and 274 ± 52 HU distal to the stent for EID, as well as 300 ± 41 HU proximal and 316 ± 55 HU for PCD, respectively. Plotted CT attenuation profiles averaged over all stents and separated by detector type visualize the smaller increase in attenuation with PCD (+188 HU, 40%) compared with the EID (+314 HU; 56%, relative difference 40%) technology (Fig. 4). Detailed quantitative results for individual stents are provided in Table 3.

DISCUSSION

This study introduces a novel photon-counting CT detector with several technical properties theoretically enabling an improved image quality and spatial resolution compared with conventional EID systems. Our study tested these aspects in a phantom with coronary artery stents of various types. We could show that the PCD array reduced blooming and improved in-stent lumen delineation, lowered image noise, and improved overall image quality.

PCD differs from current EID technology as it counts individual photons and allocates them to predetermined energy thresholds and bins based on the energy of each individual photon. The potential benefits of PCD have been investigated in various simulations and experimental studies,[17,23] achieving an in-plane spatial resolution of up to 20 lp/cm by means of 0.250 × 0.250 mm pixel size at the isocenter.[24]

To minimize confounding factors in the comparison between PCD and EID imaging, we used identical settings for tube voltage, tube current, slice thickness, matrix size, and reconstruction kernel with the same target modulation transfer function for the scans with the PCD and the EID. Still, we encountered disparities in volume CT dose index ($CTDI_{vol}$), which are, however, caused solely by penumbra effects due to differences in collimations available on the PCD and EID system. Because of the PCD's smaller beam width in the *z* axis direction, the relative contribution of the penumbra zones is larger, which explains

TABLE 3. Detailed Results by Coronary Stent*

Coronary Stent	Intraluminal Diameter, mm EID (0 degree)	Intraluminal Diameter, mm PCD (0 degree)	Intraluminal Diameter, mm EID (90 degrees)	Intraluminal Diameter, mm PCD (90 degrees)	Δ In-Stent Attenuation, HU EID (0 degree)	Δ In-Stent Attenuation, HU PCD (0 degree)	Δ In-Stent Attenuation, HU EID (90 degrees)	Δ In-Stent Attenuation, HU PCD (90 degrees)
ApoloBionert	0.8	1	0.8	0.8	542	152	92	52
CCSV	0.7	1.3	0.8	1.1	458	143	150	84
CoroflexDelta	0.7	0.9	0.8	0.9	585	570	166	133
MagicWallstent	1.2	1.2	1.2	1.2	142	64	236	231
MSM	0.6	0.9	0.7	0.8	452	263	127	106
NIR Royal	0.5	0.7	0.6	0.8	106	9	321	189
NIR Royal Adv	0.3	0.6	0.7	0.6	71	244	671	334
Palmaz	0.7	0.9	0.7	0.7	198	131	173	145
Pixel	0.7	0.9	0.8	0.8	135	150	93	77
Pura AL16	0.8	0.9	0.8	0.9	120	113	90	63
R-Stent	0.7	0.9	0.8	0.8	273	111	99	64
SonicBX	0.4	0.5	0.6	0.7	199	80	249	187
Syncro	0.7	0.7	0.8	0.8	200	115	99	55
Tecnic	0.4	0.6	0.7	0.8	124	199	164	64
Tetra	0.5	0.7	0.8	0.9	241	158	108	83
Ultra	0.5	0.6	0.6	0.7	79	30	268	167
VisionMultiLink	0.7	0.7	0.7	0.7	254	42	95	48
ZoMaxx	0.9	1.3	0.8	0.9	404	236	286	188

*Averaged results from 2 readers. EID, energy-integrating detector; PCD, photon-counting detector.

the higher $CTDI_{vol}$ compared with the EID. Most importantly, the energy dose in the images is the same for both scans. Therefore, doing the comparison at a matched tube voltage and tube current-time product is well justified for this study.

We found that the higher intrinsic spatial resolution of the PCD directly converted into noise reduction. In addition, overall image quality profits from the higher sampling rate (smaller pixels) of the PCD. Because of the improved in-plane and through-plane sampling (smaller detector pixels), images from the PCD show less pronounced nonlinear partial volume and sampling artifacts. The benefits of the PCD system are reflected in our study results, indicating a better delineation of the in-stent lumen. Still, we found better in-stent lumen visualization at a phantom position of 0 degree, suggesting a higher in-plane compared with through-plane resolution. This could be also related to the reconstructed slice width of 0.6 mm for both the PCD and EID system, potentially precluding improved in-stent lumen visualization for the PCD at 90 degrees.

There are specific technical problems when imaging coronary stents with CT. These include metal artifacts, blooming, photon starvation, beam hardening, and partial volume effects. Initial efforts in coronary stent lumen visualization were made with 16-slice CT. However, the lumen could be visualized in only approximately 54% of stents.[25,26] Gilard et al[27] showed that larger stents allowed for a better assessability of the stent lumen. Correspondingly, the sensitivity for detecting ISR with 16-slice CT increased from 54% in stents with a diameter of 3 mm or smaller to 86% in stents 3 mm or larger.[25,28] The next CT scanner development included 64-slice CT systems with higher spatial and temporal resolution. Still, limitations of CT imaging of coronary stents were found, with an artificial lumen narrowing in the range of 10% to 60%, depending on the stent characteristics.[29,30] Furthermore, recent advantages in detector technology and iterative reconstruction algorithms enabled a further improvement in through-plane resolution to 0.5 mm, being associated with a further improvement of in-stent lumen visualization.[20] Similarly, monoenergetic extrapolations from dual-energy CT with high energies and stent-specific reconstruction kernels were promising developments for improving stent imaging with CT.[31] In our study, we directly compared the most recent PCD development with the best available detector technology used for clinical routine. By doing so, we observed best results for PCD technology at 0-degree phantom position with markedly improved image quality, 16% better in-stent lumen visualization, and less blooming and partial volume artifacts, reflected in a 37% lower increase in in-stent lumen attenuation.

As mentioned previously, the PCD technology is not yet commercially available and remains of investigational nature. This holds true also for the following 2 technical limitations of the system. First, the temporal resolution of the prototype is limited by the fastest possible rotation time (currently 0.5 second). Second, the experimental PCD CT scanner does not allow for ECG support. Still, both these aspects did not interfere with the results of this study.

We acknowledge the following study limitations. First, this was an in vitro study with inherent limitations. Second, we included a relatively low number of coronary stents and did not include drug-eluting stents of the most recent generation. However, stent materials and dimensions used in our study are comparable to those currently used, so that we believe our results to be representative. Our study represents the first proof of principle with robust results on a novel detector system for CT imaging. General inferences on the limitations of the technique need to be validated in larger, prospective trials. Third, we did not evaluate the accuracy of the PCD system to detect and quantify ISR. Moreover, we did not compare different energy bins but used PCD images at the lower threshold of 25 keV instead. These images contain the entire energy spectrum, comparable to those of conventional EID images. Finally, to compare identical settings between PCD and EID, we

did not utilize an optimized stent reconstruction kernel for PCD. Novel stent-specific reconstruction kernels may advance spatial resolution in PCD imaging further.

In conclusion, our phantom study indicates the feasibility and improved quality of a novel PCD system, which might overcome previous problems of in-stent lumen visualization. Future studies should try to make full use of the PCD system in terms of spatial resolution for maximizing image sharpness using dedicated reconstruction kernels.

REFERENCES

1. Prasad A, Herrmann J. Myocardial infarction due to percutaneous coronary intervention. *N Engl J Med*. 2011;364:453–464.
2. Stefanini GG, Holmes DR Jr. Drug-eluting coronary-artery stents. *N Engl J Med*. 2013;368:254–265.
3. Serruys PW, Unger F, Sousa JE, et al. Comparison of coronary-artery bypass surgery and stenting for the treatment of multivessel disease. *N Engl J Med*. 2001;344:1117–1124.
4. Kokkinidis DG, Waldo SW, Armstrong EJ. Treatment of coronary artery in-stent restenosis. *Expert Rev Cardiovasc Ther*. 2017;15:191–202.
5. Chandrasekar B, Doucet S, Bilodeau L, et al. Complications of cardiac catheterization in the current era: a single-center experience. *Catheter Cardiovasc Interv*. 2001;52:289–295.
6. Wintersperger BJ, Bamberg F, De Cecco CN. Cardiovascular imaging: the past and the future, perspectives in computed tomography and magnetic resonance imaging. *Invest Radiol*. 2015;50:557–570.
7. Lell MM, Wildberger JE, Alkadhi H, et al. Evolution in computed tomography: the battle for speed and dose. *Invest Radiol*. 2015;50:629–644.
8. Runge VM, Marquez H, Andreisek G, et al. Recent technological advances in computed tomography and the clinical impact therein. *Invest Radiol*. 2015;50:119–127.
9. Habbel C, Hetterich H, Willner M, et al. Ex vivo assessment of coronary atherosclerotic plaque by grating-based phase-contrast computed tomography: correlation with optical coherence tomography. *Invest Radiol*. 2017;52:223–231.
10. Hetterich H, Willner M, Habbel C, et al. X-ray phase-contrast computed tomography of human coronary arteries. *Invest Radiol*. 2015;50:686–694.
11. Schroeder S, Achenbach S, Bengel F, et al. Cardiac computed tomography: indications, applications, limitations, and training requirements: report of a Writing Group deployed by the Working Group Nuclear Cardiology and Cardiac CT of the European Society of Cardiology and the European Council of Nuclear Cardiology. *Eur Heart J*. 2008;29:531–556.
12. Authors/Task Force m, Windecker S, Kolh P, et al. 2014 ESC/EACTS Guidelines on myocardial revascularization: The Task Force on Myocardial Revascularization of the European Society of Cardiology (ESC) and the European Association for Cardio-Thoracic Surgery (EACTS) Developed with the special contribution of the European Association of Percutaneous Cardiovascular Interventions (EAPCI). *Eur Heart J*. 2014;35:2541–2619.
13. Taylor AJ, Cerqueira M, Hodgson JM, et al. ACCF/SCCT/ACR/AHA/ASE/ASNC/NASCI/SCAI/SCMR 2010 appropriate use criteria for cardiac computed tomography. A report of the American College of Cardiology Foundation Appropriate Use Criteria Task Force, the Society of Cardiovascular Computed Tomography, the American College of Radiology, the American Heart Association, the American Society of Echocardiography, the American Society of Nuclear Cardiology, the North American Society for Cardiovascular Imaging, the Society for Cardiovascular Angiography and Interventions, and the Society for Cardiovascular Magnetic Resonance. *J Am Coll Cardiol*. 2010;56:1864–1894.
14. Leng S, Gutjahr R, Ferrero A, et al. Ultra-high spatial resolution, multi-energy CT using photon counting detector technology. *Proc SPIE Int Soc Opt Eng*. 2017;10132.
15. Leng S, Yu Z, Halaweish A, et al. Dose-efficient ultrahigh-resolution scan mode using a photon counting detector computed tomography system. *J Med Imaging (Bellingham)*. 2016;3:043504.
16. Yu Z, Leng S, Jorgensen SM, et al. Evaluation of conventional imaging performance in a research whole-body CT system with a photon-counting detector array. *Phys Med Biol*. 2016;61:1572–1595.
17. Pourmorteza A, Symons R, Sandfort V, et al. Abdominal imaging with contrast-enhanced photon-counting CT: first human experience. *Radiology*. 2016;279:239–245.
18. Symons R, Cork TE, Sahbaee P, et al. Low-dose lung cancer screening with photon-counting CT: a feasibility study. *Phys Med Biol*. 2017;62:202–213.
19. Gutjahr R, Halaweish AF, Yu Z, et al. Human imaging with photon counting-based computed tomography at clinical dose levels: contrast-to-noise ratio and cadaver studies. *Invest Radiol*. 2016;51:421–429.
20. von Spiczak J, Morsbach F, Winklhofer S, et al. Coronary artery stent imaging with CT using an integrated electronics detector and iterative reconstructions: first in vitro experience. *J Cardiovasc Comput Tomogr*. 2013;7:215–222.
21. Seifarth H, Ozgun M, Raupach R, et al. 64- Versus 16-slice CT angiography for coronary artery stent assessment: in vitro experience. *Invest Radiol*. 2006;41:22–27.
22. Landis JR, Koch GG. The measurement of observer agreement for categorical data. *Biometrics*. 1977;33:159–174.
23. Shikhaliev PM. Energy-resolved computed tomography: first experimental results. *Phys Med Biol*. 2008;53:5595–5613.
24. Leng S, Yu Z, Halaweish A, et al. A high-resolution imaging technique using a whole-body, research photon counting detector ct system. *Proc SPIE Int Soc Opt Eng*. 2016;9783.
25. Maintz D, Seifarth H, Flohr T, et al. Improved coronary artery stent visualization and in-stent stenosis detection using 16-slice computed-tomography and dedicated image reconstruction technique. *Invest Radiol*. 2003;38:790–795.
26. Mahnken AH. CT imaging of coronary stents: past, present, and future. *ISRN Cardiol*. 2012;2012:139823.
27. Gilard M, Cornily JC, Pennec PY, et al. Assessment of coronary artery stents by 16 slice computed tomography. *Heart*. 2006;92:58–61.
28. Mahnken AH, Buecker A, Wildberger JE, et al. Coronary artery stents in multislice computed tomography: in vitro artifact evaluation. *Invest Radiol*. 2004;39:27–33.
29. Maintz D, Seifarth H, Raupach R, et al. 64-slice multidetector coronary CT angiography: in vitro evaluation of 68 different stents. *Eur Radiol*. 2006;16:818–826.
30. Maintz D, Burg MC, Seifarth H, et al. Update on multidetector coronary CT angiography of coronary stents: in vitro evaluation of 29 different stent types with dual-source CT. *Eur Radiol*. 2009;19:42–49.
31. Hickethier T, Baessler B, Kroeger JR, et al. Monoenergetic reconstructions for imaging of coronary artery stents using spectral detector CT: In-vitro experience and comparison to conventional images. *J Cardiovasc Comput Tomogr*. 2017;11:33–39.